Design and development of lightweight Fe-Mn alloys for storage and transportation of liquified natural gas (LNG) — Computational materials modelling study

by M. Phasha, L. Mampuru, D. Mkhonto, J. Moema

Affiliation:
Advanced Materials Division, Mintek, South Africa

Correspondence to:
M. Phasha

Email:
majep@mintek.co.za

Dates:
Received: 15 Oct. 2025
Published: March 2025

How to cite:
Phasha, M., Mampuru, L., Mkhonto, D., Moema, J. 2025. Design and development of lightweight Fe-Mn alloys for storage and transportation of liquified natural gas (LNG) — Computational materials modelling study. *Journal of the Southern African Institute of Mining and Metallurgy*, vol. 125, no. 3, pp. 145–150

DOI ID:
https://doi.org/10.17159/2411-9717/761/2025

ORCiD:
M. Phasha
http://orcid.org/0000-0003-4295-9247
L. Mampuru
http://orcid.org/0000-0003-2009-2665
D. Mkhonto
http://orcid.org/0000-0003-0329-8095
J. Moema
http://orcid.org/0000-0002-9517-9749

This paper is based on a presentation given at the Mintek@90 Conference 2024, 11-12 November 2024, Sandton Convention Centre, Johannesburg, South Africa

Abstract

The global liquified natural gas (LNG) storage market size is projected to reach USD17.5 billion by 2025. Currently, owed to its high toughness, tensile strength, and excellent weldability, the 9% nickel steel is the most used in building infrastructure for cryogenic applications such as the construction of tanks and pipes for storage and transportation of LNG. However, this alloy is not readily available because of its complex production process and high cost. This provides an opportunity for suitable alternative materials to build infrastructure for cryogenic applications. Among strong contenders is the Fe-Mn based alloys, which have sparked global interest due to their desirable properties such as relatively lower density, low cost, high toughness and strength, due to a high manganese (Mn) content. These attractive properties render Fe-Mn based alloys preferred candidates to replace traditional steels in engineering applications in which strength-weight ratio is critical. In response, as a build-up to designing and developing austenitic Fe-Mn alloys, the present study employed density functional theory (DFT) based first-principles computational materials modelling technique to investigate the structural, thermodynamic, and magnetic properties of binary Fe-Mn alloy composition in competing FCC, HCP, and BCC crystal structures. Using this approach, it was possible to unravel the key underlying elastic properties that are directly correlated to experimental tensile strength and high toughness in binary Fe-Mn alloys. Besides successfully validating the existing experimental data, the current predicted properties and the deployed approach will serve as a benchmark from which further alloying required to improve other properties will be conducted.

Keywords

liquefied natural gas, 9% nickel steel, binary Fe-Mn alloys, first-principles calculations

Introduction

In the quest to meet the greenhouse gas (GHG) emission targets set out in the Paris Agreement (2015), there is worldwide exploration of viable sustainable and environmentally friendly energy options, aimed at the effective curbing of global warming. Amongst alternative, relatively cleaner energy sources that have attracted much attention in the effort to diversify energy supply in what is termed 'energy-mix', is the liquified natural gas (LNG). The global LNG storage market size is projected to reach USD17.5 billion by 2025 (GlobalEnergyWorld, 2020). Storage and distribution of LNG is conducted at a cryogenic temperature of -196 °C (77 K). As a result, very few commercial alloys are able to withstand such sub-zero temperatures while maintaining the required impact toughness of 100 J. Currently, owing to their high toughness, tensile strength, and excellent weldability, the 6–9% nickel (Ni) steel alloys are the most used in building infrastructure for cryogenic environment (77 K) applications such as the construction of tanks and pipes for storage and transportation of LNG (Hickmann, et al. 2005, Kim, et al.2021) . The most successful and readily available being the 9% Ni steel alloy that is comprised of face-centred-cubic (FCC) and body-centred-cubic (BCC) dual phase microstructure and referred to as γ+α or γ+α´. Although the undesired ε-hexagonal-close-packed (HCP) martensite that is detrimental to toughness forms upon forging due to small stacking fault energy (SFE), it is eliminated by applying an appropriate heat treatment process in the γ+α region. However, this material is not readily available because of its complex production process and high cost of Ni. This poses an opportunity for suitable alternative alloyed materials to build infrastructure for such cryogenic environments. Among the strong frontrunners in this pursuit are the Fe-Mn based alloys that have sparked global interest in many engineering applications due to their desirable properties such as lower density than traditional steels,

low cost, high toughness and strength, due to the high manganese (Mn) content (Kim et al., 2021; Lee et al., 2014; Sohn et al., 2015; Chowdhury et al., 2017; Guerrero et al., 2017; Bleck and Haase, 2019; Bastidas et al., 2021). These attractive properties render Fe-Mn based alloys preferred candidates to replace traditional steels in engineering applications in which strength-weight ratio is critical. Moreover, South Africa endows high-grade iron (Fe) ore and is home to more than 70% of the global Mn ore reserves (U.S. Geological Survey, 2020). Consequently, the development of Fe-Mn based alloys is seen as a great downstream beneficiation opportunity capable of not only unlocking, but also stimulating local economic growth.

As a build-up to designing and developing dual phase Fe-Mn alloys consisting of FCC (γ)+BCC (α or α′) crystal structures, the present study employed the ab initio computational materials modelling technique to generate structural, thermodynamic, and magnetic properties of binary competing FCC, HCP, and BCC Fe-Mn phases in various alloy compositions. In addition, the elastic properties of non-magnetic (NM) FCC and ferromagnetic (FM) BCC Fe-Mn alloy compositions are presented. Using this computational tool, that has become more reliable in predicting properties of solids, it was possible to identify compositions and elastic properties that can be linked to yield strength and high toughness at cryogenic temperature (0 K). Similar studies on binary Fe-Mn alloys have previously been carried out, however, the focus was on the structural and thermodynamic properties (Gebhardt et al., 2010 ; Lintzen et al., 2013) with very limited research on magnetic (Gebhardt et al., 2010) and elastic properties. Thus, in the current study, the first-principles calculations were conducted to generate structural, thermodynamic, and magnetic property data of binary FCC, HCP and BCC Fe-Mn alloys using the supercell approach. In some cases, the elasticity data for cubic Fe-Mn alloy compositions is also presented. The overal intent of this work is to unravel the key underlying properties of various Fe-Mn alloy compositions that could be directly correlated to available experimental data for validation purposes.

Methodology

All calculations reported in this study were performed on 2x2x2 FCC, HCP, and BCC supercells comprised of 32, 16 and 16 atoms, respectively, to represent $Fe_{1-x}Mn_x$ alloy compositions from $Fe_{32-x}Mnx$ and $Fe_{16-x}Mn_x$ supercells. This work was carried out using the density functional theory (DFT)-based CASTEP code embedded in the Materials Studio software package (Clark et al., 2005). The robust Vanderbilt ultrasoft pseudopotentials (Vanderbilt, 1990) were used to describe the ion-electron interaction within the generalised gradient approximation (GGA) (Perdew and Wang, 1992) with PW91 functional (Perdew et al., 1992), with spin polarisation (SP) for FCC, HCP, and BCC as well as the non-spin polarisation (NSP) for FCC (NM) Fe-Mn alloy compositions. A plane wave cutoff energy of 500 eV and k-points set of 6x6x6, 12x12x6, 8x8x8, and 8x8x8 were sufficient to converge the total energy of the considered system in a non-magnetic state. The ground-state structures were optimised using the Broyden-Fletcher-Goldfarb-Shanno (BFGS) minimisation scheme. The convergence criterion of less than 1×10^{-5} eV/atom, the maximum residual forces of 0.03 eV/Å, maximum residual bulk stress of 0.05 GPa and maximum atomic displacement of 1×10^{-3} Å were utilised.

Phase stability

The heat of formation calculated using Equation 1 was used to determine the thermodynamic stability of the alloy compositions considered in this study:

$$H_F^{Alloy} = \frac{1}{n}E_{Total}^{Alloy} - [1 - xE_{Solid}^{Fe} + xE_{Solid}^{Mn}] \quad [1]$$

where E_{Total}^{Alloy} is the total energy of the alloy composition, E_{Solid}^{Fe} and E_{Solid}^{Mn} are the total energies of the ground-state structures of elemental Fe and Mn, respectively, whereas x and 1 - x refer to the fractional concentrations of the constituent elements; the total number of atoms in the structure is represented by n.

Elastic properties

The stress-strain relation may be used to distinguish the elastic and plastic regimes of solid materials. The elastic moduli are the fundamental physical parameters that establish the stress-strain relation in the elastic regime. For an isotropic polycrystalline solid, the two independent elastic parameters are the bulk modulus (B) and the trigonal shear modulus (G). The ratio of B/G predicts the brittleness of metals, depending on the threshold value of 1.75 (ductile if above 1.75) (Pugh, 1954). These elastic moduli are calculated from elastic constants computed from applying an appropriate set of strains to the geometrically relaxed unit cell. Elastic constants are then determined from the resulting change in total energy on the deformation. For the cubic structures, there are only three independent elastic constants, namely, C_{11}, C_{12}, and C_{44}. The mechanical stability criteria for a cubic crystal is given by the expressions in Equations 2 and 3:

$$C_{11} > 0,\ C_{44} > 0,\ C_{11} - C_{12} > 0,\ C_{11} + 2C_{12} > 0 \quad [2]$$

$$B = \frac{1}{3}(C_{11} + 2C_{12}),\ C' = \frac{C_{11}-C_{12}}{2},\ E = \frac{9BG}{3B+G},\ \nu = (3B - E)/6B \quad [3]$$

where E is the modulus of elasticity, C the tetragonal shear modulus, and Poisson's ratio ν.

Results and discussion

Phase stability

The lattice constants of the geometrically relaxed FCC, HCP, and BCC crystal structures of considered binary Fe-Mn alloy compositions are presented in Table 1. As a consequence of Mn having slightly larger atomic radius than Fe, the lattice constant a_0 of all phases increases gradually with an increase in Mn composition, as observed in Table 1. However, for FCC Fe-Mn alloy compositions in AFM state, the increase is a bit rapid until at 15.625 at.% Mn, followed by fluctuation thereafter, while the increase in lattice constant of FCC (NM) is linear. This anomaly could be attributed to non-linear antiferromagnetic behaviour, as is demonstrated in Figure 1. With the exception of FCC (AFM), the lattice constant trends established in this work are similar to those of theoretical results reported by and experimental data therein. This is the case, despite the fact that the lattice constants predicted in the current study are much smaller, in agreement with other predicted results (Bleskov et al., 2016) and in line with the experimentally observed lattice contraction in BCC Fe (FM→NM) upon heating, prior to α→γ phase transition. According to the present authors, it is this lattice contraction that is responsible for the onset non-magnetic Fe.

Table 1

Equilibrium lattice constants of binary FCC, HCP and BCC Fe-Mn alloy compositions

Mn composition	FCC (NM)	FCC (AFM)	HCP (NM)	BCC (FM)
(atomic %)	Lattice constant a_0 (Å)			
0	3.4348	3.4348	2.4494 c/a =1.5833	2.8112
6.25	3.4425	3.4456	2.4542 c/a =1.5832	2.8130
12.5	3.4489	3.4940	2.4721 c/a =1.5932	2.8131
15.625	3.4522	3.5051	-	-
18.75	3.4544	3.4597	2.4626 c/a =1.5843	2.8144
21.875	3.4585	3.5204	-	-
25	3.4606	3.4604	2.4712 c/a =1.5876	2.8155

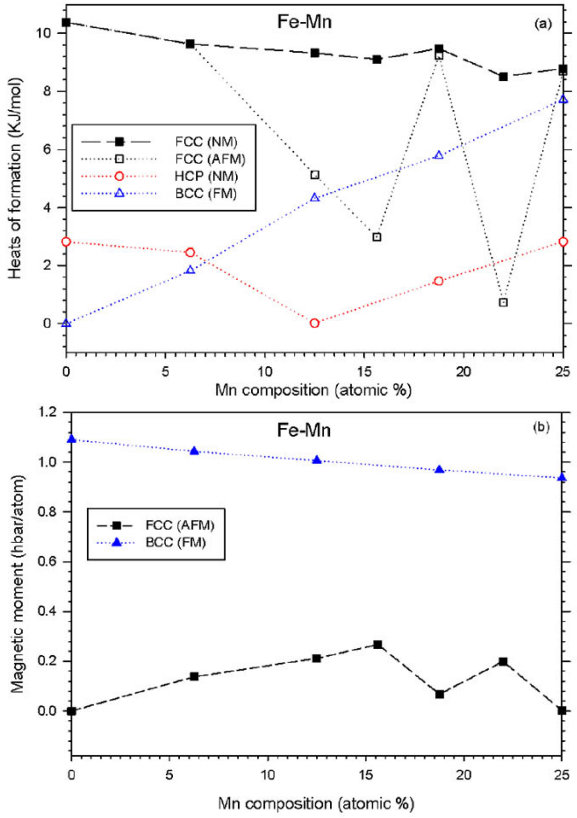

Figure 1—The calculated (a) heats of formation for FCC, HCP and BCC as well as (b) magnetic moments of FCC (AFM) and BCC (FM) binary Fe-Mn alloy compositions

The heat of formation of considered binary Fe-Mn alloy compositions in FCC, HCP, and BCC crystal structures, as well as the corresponding magnetic moments of FCC (AFM) and BCC (FM) phases are presented in Figures 1(a) and (b), respectively. It is evident from Figure 1(a) that the austenitic (FCC) Fe-Mn alloy compositions are the least thermodynamically stable at lower Mn compositions ≤ 12.5 at.%. This is in accordance with literature (Okamoto, 1992), as BCC (FM) remains the most stable from 0 to just below 7 at.% Mn, after which the HCP phase is dominant for a broad range of compositions with highest stability 12.5 at.% Mn. The HCP (NM) phase is in competition with FCC (AFM) only at 15.625% and 21.875.% Mn in terms of stability, with FCC (AFM) being the most stable at 21.875.% Mn. On the other hand, the stability of BCC (FM) decreases sharply with an increase in Mn composition. The current predicted phase stability trends are in excellent agreement with other theoretical predictions (Lintzen et al., 2013). As shown in Figure 1(b), it is worth noting that the FCC (AFM) has the highest magnetic moments at the aforementioned two Mn compositions with higher thermodynamic stability. The magnetic moment is zero at 0, 18.75 and 25 at.% Mn, the compositions at which the thermodynamic stability is the lowest. On the other hand, although it remains strongly magnetic, the magnetic moments of BCC (FM) reduce gradually with an increase in Mn composition.

The driving force behind the key deformation mechanisms such as transformation-induced plasticity (TRIP) and twinning-induced plasticity (TWIP) in the high-Mn steels is the stacking fault energy (SFE) (Welsch et al., 2016). It is reported that TRIP is dominant at low SFE (< 20 mJ^{-2}), whereas TWIP occurs if SFE is much higher to suppress any possible martensitic transformation. Since the SFE corresponds directly to FCC-HCP phase transition, it is therefore directly proportional to the total energy difference between these two phases. Hence, due to its strong influence on the hardening mechanisms in Fe-Mn alloys, the calculated structural energy difference between FCC and HCP is plotted against Mn composition in Figure 2. Clearly, there is not much in energy difference when FCC is at NM or AFM state with respect to the HCP phase, except at 12.5 at.% Mn composition where there a significant polarised difference with FCC (NM) enjoying the largest energy difference to HCP than FCC (AFM). However, the predicted energy difference trend is not so linear as others have reported (Gebhardt et al., 2010 ; Guerrero et al., 2020).

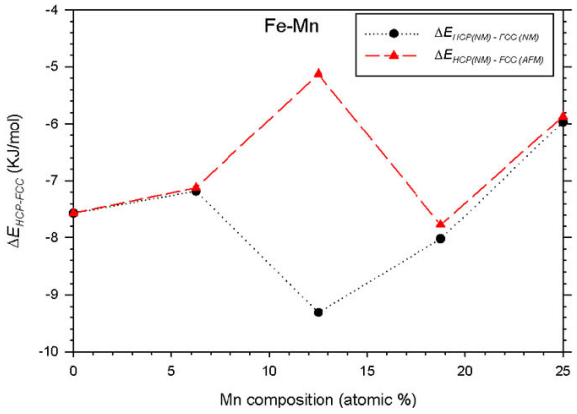

Figure 2—The structural energy difference between FCC and HCP binary Fe-Mn alloy compositions

Elastic properties

The calculated elastic constants of the binary FCC (NM) and BCC (FM) Fe-Mn alloy compositions are presented in Tables 2 and 3, respectively. As shown in Table 2, in general, the increase in Mn composition results in a gradual decrease in C_{11} and C_{44} elastic constants while there is a slight increase in C_{12}. The resulting elastic moduli (C', B, and E) also decrease with an increase in Mn composition although the decrease in bulk modulus is very small. In accordance with the Hall-Petch effect, it is evident from Tables 2 and 3, that the Young's modulus (E) values of polycrystalline alloys are much higher than that of the single crystalline counterpart due to grain-size strengthening effect (Cordero et al., 2016). This results in a larger value of the trigonal shear modulus (G) calculated using an expression, as expressed in Equation 4. Subsequently, the B/G ratio decreases leading to a smaller Poisson's ratio (ν), both indicative of reduction in ductility. Thus, the mechanical properties of single crystal material may be viewed as the lower bound whereas those of polycrystalline material are upper bound. For example, single crystal FCC Fe is predicted to be ductile as the values of B/G ratio and Poisson's ratio (ν) are all far above threshold values of 1.75 and 0.26, respectively. However, its polycrystalline counterpart may become brittle if the lowest values of 1.65 and 0.2478 for B/G and

Table 2

Computed elastic properties of FCC (NM) Fe-Mn alloy compositions

Mn comp.	Crystal-type	Elastic constants C_{ij} (GPa)			Elastic moduli (GPa)			Pugh's ratio	Poisson's ratio
		C_{11}	C_{12}	C_{44}	C'	B	E	B/G	ν
0	S-cryst.	463	233	260	115	310	307	2.69	0.3348
	P-cryst						468	1.65	0.2478
6.25	S-cryst.	445	237	254	104	307	280	2.95	0.3478
	P-cryst						446	1.73	0.2570
12.5	S-cryst.	439	239	253	100	305	270	3.06	0.3524
	P-cryst						439	1.75	0.2600
18.75	S-cryst.	431	242	247	95	305	257	3.23	0.3595
	P-cryst						426	1.82	0.2670
25	S-cryst.	422	248	243	87	306	238	3.53	0.3705
	P-cryst.						411	1.90	0.2760

Table 3

Computed elastic properties of BCC (FM) Fe-Mn alloy compositions

Mn comp.	Crystal-type	Elastic constants C_{ij} (GPa)			Elastic moduli (GPa)			Pugh's ratio	Poisson's ratio
		C_{11}	C_{12}	C_{44}	C'	B	E	B/G	ν
0	S-cryst.	307	163	127	72	211	193	2.93	0.3474
	P-cryst.						261	2.09	0.2870
6.25	S-cryst.	310	176	134	67	221	182	3.30	0.3624
	P-cryst.						264	2.18	0.3000
12.5	S-cryst.	311	186	134	62	228	172	3.65	0.3745
	P-cryst.						259	2.31	0.3110
18.75	S-cryst.	310	194	144	58	232	160	4.02	0.3851
	P-cryst.						262	2.33	0.3120
25	S-cryst.	301	197	145	52	231	145	4.45	0.3955
	P-cryst.						253	2.41	0.3180

Poisson's ratio (v), respectively, are reached by obtaining smallest grains. It is evident from Table 2 that as materials'

$$G = \frac{3BE}{9B-E} \quad [4]$$

stiffness (E) decreases with the addition of Mn, the ductility increases, as shown by B/G and Poisson's ratios. Polycrystalline FCC (NM) starts to be ductile upon adding 12.5 at.% Mn. On the other hand, due to its soft nature, the stiffness (E) of all considered BCC (FM) Fe-Mn alloy compositions in both single crystal and polycrystalline states is much smaller than even the single crystal of FCC (NM). Thus, BCC phase will be key to ensure toughness while FCC phase will provide strength, a property combination required in dual phase Fe-Mn alloys. Therefore addition of Mn much higher than 12.5 at.% will not only ensure that the ductile to brittle transition (DBT) is suppressed at cryogenic temperature but provides room for solid-solution-strengthening of FCC Fe-Mn alloys by adding other alloying in an attempt to increase its stiffness (E), which is directly proportional to yield strength as well as improving its thermodynamic stability.

Conclusions

First-principles calculations were successfully conducted to generate structural, thermodynamic, and magnetic property data of binary FCC, HCP, and BCC Fe-Mn alloys using the supercell approach. In general, the predicted equilibrium lattice constants increased slightly with an increased Mn composition. The highest thermodynamic stability is obtained at Fe-Mn alloy compositions with 12.5 and 21.875 at.% Mn for HCP and FCC (AFM) phases, respectively. An increase in magnetic moment seem to influence the thermodynamic stability of FCC (AFM) phase. While the thermodynamic stability of ferromagnetic BCC Fe-Mn decreases sharply with an increase in Mn composition, its magnetic strength drops gradually. The trends for structural energy difference between FCC and HCP phases of binary Fe-Mn alloy compositions are not linear, as reported elsewhere. Elasticity data reveal that a minimum of 12.5 at.% Mn is required to meet the minimum ductility threshold in FCC (NM) Fe-Mn alloys, while the BCC (FM) alloys maintain its soft character shown by lower Young's modulus (stiffness) and high ductility indicated by B/G and v values way higher than the threshold values. Thus, BCC phase will be key to ensure toughness while FCC phase will provide strength, a property combination required in dual phase Fe-Mn alloys. Therefore addition of Mn much higher than 12.5 at.% will not only ensure that the ductile to brittle transition (DBT) is suppressed at cryogenic temperature, but provides room for solid-solution-strengthening of FCC Fe-Mn alloys by adding other alloying in an attempt to increase its stiffness (E), which is directly proportional to yield strength as well as improving its thermodynamic stability.

Acknowledgements

The authors would like to thank MINTEK and the Advanced Metals Initiative (AMI) of the Department of Science and Innovation (DSI) for financial support. Gratitude is also extended to the Centre for High-Performance Computing (CHPC) in Cape Town for allowing us to carry out the calculations using their remote computing resources.

References

GlobalEnergyWorld. 2020. https://www.globalenergyworld.com/news/traditional-energy [accessed 27 Feb 2020].

Hickmann, K., Kern, A., Schriever, U., Stumpfe, J. 2005. Production and properties of high strength nickel alloy steel plate for low temperature applications. ThyssenKrupp Stahl AG, Division Metallurgy/Heavy Plate, Profit Center Heavy Plate, Germany.

Kim, T-Y., Yoon, S-W., Kim, J-H., Kim, M-H. 2021. Fatigue and Fracture Behavior of Cryogenic Materials Applied to LNG Fuel Storage Tanks for Coastal Ships. *Metals*, vol. 11, no. 1899.

Lee, J., Sohn, S.S., Hong, S., Suh, B-C., Kim, S-K., Lee, B-J., Kim, N.J., Lee, S. 2014. Effects of Mn Addition on Tensile and Charpy Impact Properties in Austenitic Fe-Mn-C-Al-Based Steels for Cryogenic Applications. *Metallurgical and Materials Transactions*. A, vol. 45, no. 5419.

Sohn, S.S., Hong, S., Lee, J., Suh, B-C., Kim, S-K., Lee, B-J., Kim, N.J., Lee, S. 2015. Effects of Mn and Al contents on cryogenic-temperature tensile and Charpy impact properties in four austenitic high-Mn steels. *Acta Materialia*, vol. 100, no. 39.

Chowdhury, P., Canadinc, D., Sehitoglu, H. 2017. On deformation behavior of Fe-Mn based structural alloys. *Materials Science and Engineering R*, vol. 122, no. 1.

Guerrero, L.M., La Roca, P., Malamud, F., Baruj, A., Sade, M. 2017. Composition effects on the fcc-hcp martensitic transformation and on the magnetic ordering of the fcc structure in Fe-Mn-Cr alloys. *Materials Design*, vol. 116, no. 127.

Bleck, W., Haase, C. 2019. Physical Metallurgy of High Manganese Steels. *Metals,* vol. 9, no. 1053.

Bastidas, D.M., Ress, J., Bosch, J., Martin, U. 2021. Corrosion Mechanisms of High-Mn Twinning-Induced Plasticity (TWIP) Steels: A Critical Review. *Metals*, vol. 11, no. 287.

U.S. Geological Survey. 2020. Mineral commodity summaries 2020 U.S. Geological Survey, 200, https://doi.org/10.3133/ mcs2020

Gebhardt, T., Music, D., Hallstedt, B., Ekholm, M., Abrikosov, I.A., Vitos, L., Schneider, J.M. 2010. Ab initio lattice stability of fcc and hcp Fe–Mn random alloys. *Journal of Physics: Condensed Matter*, vol. 22, no. 295402.

Lintzen, S., Von Appen, J., Hallstedt, B., Dronskowski, R. 2013. The Fe–Mn enthalpy phase diagram from first principles. *Journal of Alloys and Compounds*, vol. 577, no. 370.

Clark, S., Segall, M.D., Pickard, C.J., Hasnip, P.J., Probert, M.J., Refson, K., Payne, M.C. 2005. First principles methods using CASTEP. *Zeitschrift für Kristallographie*, vol. 220, no. 567.

Vanderbilt, D. 1990. Soft self-consistent pseudopotentials in a generalized eigenvalue formalism. *Physical Review B*, vol. 41, no. 7892.

Paris Agreement to the United Nations Framework Convention on Climate Change, Dec. 12, 2015, T.I.A.S. No. 16-1104.

Perdew, J.P., Wang, Y. 1992. Accurate and simple analytic representation of the electron-gas correlation energy. *Physical Review B*, vol. 45, no. 13244.

Perdew, J.P., Chevary, J.A., Vosko, S.H., Jackson, K.A., Pederson, M.R., Singh, D.J., Fiolhais, C. 1992. Atoms, molecules, solids, and surfaces: Applications of the generalized gradient approximation for exchange and correlation. *Physical Review B*, vol. 46, no. 6671.

Pugh S.F. 1954. Relations between the elastic moduli and the plastic properties of polycrystalline pure metals. *Philosophical Magazine and Journal of Science*, vol. 45, no. 367, p. 823.

Bleskov I., Hickel T., Neugebauer J., Ruban A. 2016. Impact of local magnetism on stacking fault energies: A first-principles investigation for fcc iron. *Physical Review B*, vol. 93, no. 214115.

Okamoto, H. 1992. *Phase Diagrams of Binary Iron Alloys*, ASM International.

Welsch, E., Ponge, D., Hafez Haghighat, S.M., Sandlöbes, S., Choi P., Herbig, M., Zaefferer, S.D., Raabe, D. 2016. Strain hardening by dynamic slip band refinement in a high-Mn lightweight steel. *Acta Materialia*, vol. 116, no. 188.

Guerrero, L.M., La Roca, P., Malamud, F., Baruj, A., Sade, M. 2020. A Short Review on the Effect of Cr on the fcc–hcp Phase Transition in Fe–Mn-Based Alloys. *Shape Memory and Superelasticity*, vol. 6, no. 202.

Cordero, Z.C., Knight, B.E., Schuh, C.A. 2016. Six decades of the Hall–Petch effect – a survey of grain-size strengthening studies on pure metals. *International Materials Reviews*, vol. 61 no. 8, p. 495. ◆